An Analysis of the Performance of a Handset Diversity Antenna Influenced by Head, Hand, and Shoulder Effects at 900 MHz: Part I—Effective Gain Characteristics

Koichi Ogawa, *Member, IEEE,* Toshimitsu Matsuyoshi, and Kenji Monma

***Abstract*—A diversity antenna for portable telephones, which is composed of a whip antenna and a planar inverted F-antenna (PIFA) operating at 900 MHz, has been analyzed. The analysis includes the electromagnetic effects of a human operator. Wire-grid analysis yielded radiation efficiency, mean effective gain, correlation coefficient, and diversity gain characteristics under various incident wave propagation environments with whip length, head-to-radio separation, and inclination of the radio from the vertical as parameters. The analysis has been carried out using a homogeneous human phantom model, which includes a head, a hand, and a left shoulder. The description of this work is divided into two parts, devoted, respectively, to the effective gain characteristics in multipath propagation environments in Part I and to the correlation characteristics of the diversity branches in Part II. The analytical results indicate the structural and environmental requirements for designing the diversity antenna with a high diversity effect under practical use conditions.**

***Index Terms*—Body effect, correlation coefficient, diversity, effective gain, moment method, portable telephone.**

I. Introduction

With the expansion of cellular telephone services, there has been an interest in and much research directed toward antenna gain enhancement in ordinary use situations. In order to reduce multipath fadings in a land mobile communication environment, diversity reception techniques are employed for portable telephone terminals because high diversity gain can be achieved while at the same time equipment can be further miniaturized. A very compact diversity antenna configuration for portable telephones comprising a retractable whip antenna and a built-in planar inverted F-antenna (PIFA) has been developed [1]. In order to obtain high diversity, the correlation between diversity branches must be small while maintaining a high effective gain [2] in the communication environment. To this end, correlation coefficients and effective gains have been analyzed in free space in relation to antenna structures under various radiowave propagation environments [3], [24], [4], [25]. However, few theoretical analyses evaluating these relationships—which include electromagnetic interaction due to the presence of the antenna, the hand-held unit, and the human operator—have been reported. For designing a diversity antenna with a small correlation coefficient and a high effective gain, analysis of these characteristics under practical use conditions is essential.

Because portable telephones operate in proximity to the human body, one particular important consideration involves the interaction of radiant electromagnetic fields with nearby biological tissue. The operator's influence on antenna gain, radiation pattern, and input impedance has been investigated theoretically by the moment method [5], [6] and the finite difference time-domain method [7], [8], [26], [9], [10]. These studies indicate that significant gain reduction occurs when the antenna is used close to the human body, and approximately half of the transmission power is absorbed in the human body, resulting in a radiation efficiency of less than 0.5. In these analyses, human heads were modeled by a sphere [7], a cube [8], [26], a spheroid [6], or a more realistic shape [5], [9], [10].

Recently, some studies have modeled a hand holding a portable telephone [7], [8], [26], [9], [10]. The effect of the hand depends on the type of antenna used; the effect is relatively small for an external whip antenna, whereas the effect becomes significantly large for a built-in antenna when the antenna approaches the hand [8], [26], [9]. On the other hand, the shoulder is a part of the human body that can affect the antenna characteristics since the radio and the shoulder are in close proximity when the shoulder is raised in the usual talk position. In such a situation, the shoulder could provide a different effect compared to the hand because the hand is regarded as a bulky object located near the antenna, whereas the shoulder is an extended plane at a distance of approximately a quarter-wavelength at 900 MHz from the antenna. For this reason, the authors have presented a basic study of the effects of the shoulder on the impedance and radiation characteristics of a half-wavelength dipole antenna located near the head at 900 MHz [11], [27].

The purpose of this paper is to make a wire-grid analysis of a diversity antenna comprising a whip antenna and a built-in PIFA, to include the electromagnetic effects of a human operator and to evaluate diversity performance with regard to the whip length, the head-to-radio separation, and the radio inclination angle from the vertical under various multipath propagation environments. The analysis has been carried out by the use of a homogeneous human phantom model, which includes a head,

Manuscript received August 13, 1998; revised March 21, 2000.

The authors are with the Devices Development Center, Matsushita Electric Industrial Company, Ltd., Osaka 571-8501, Japan.

Publisher Item Identifier S 0018-9545(01)03226-1.

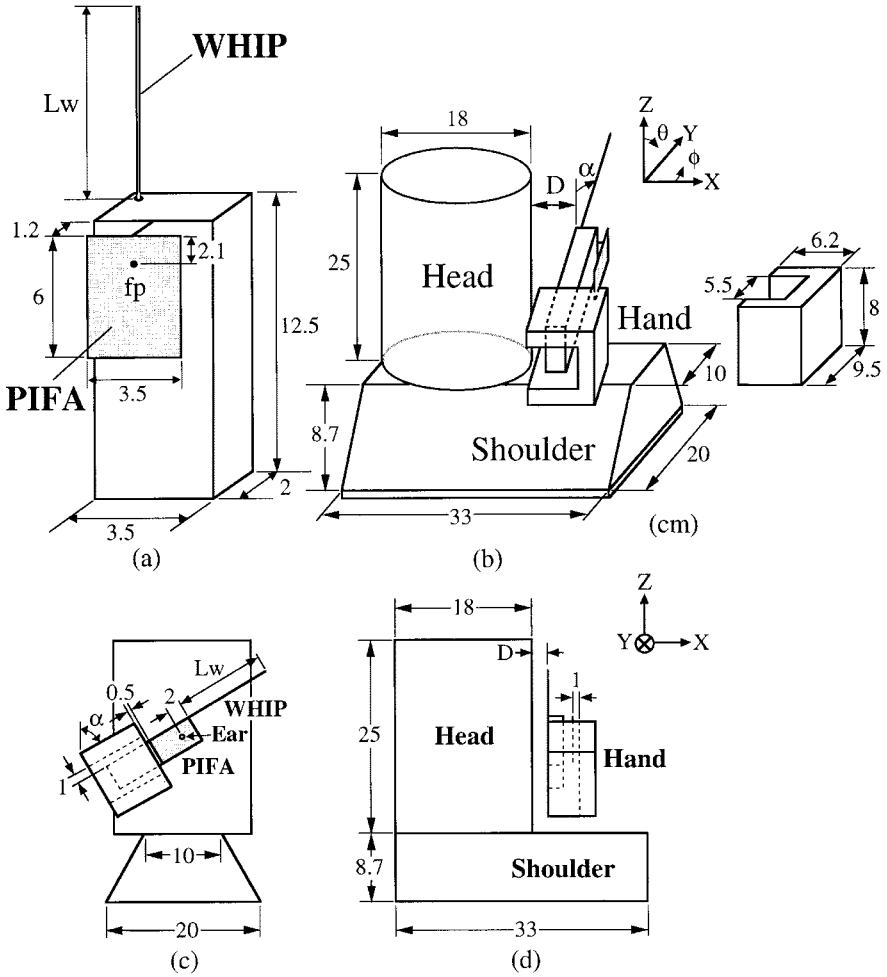

Fig. 1. (a) Configuration of the diversity antenna, (b) outline of the human model, (c) side view, and (d) front view.

a hand, and a left shoulder. The description of this work is divided into two parts, devoted, respectively, to the effective gain characteristics in multiple radiowave propagation environments in Part I and to the correlation characteristics of the diversity branches in Part II. The analytical results indicate the structural and environmental requirements for designing the diversity antenna with a high diversity effect under practical use conditions.

This paper (Part I) first presents the configuration of the diversity antenna and the wire-grid model in Section II. Equations for calculating the radiation efficiency and the effective gain, and a theoretical model for the incident wave distribution, are presented. In addition, simultaneous conjugate-matched conditions for the two antennas, as is the usual case for commercial portable telephones, are discussed. The effects of a shoulder on the radiation and effective gain characteristics are discussed in Section III. In that discussion, there is a demonstration of how the characteristics of whip antennas of different whip lengths and the PIFA are changed by the proximity of a shoulder. In Section IV, the calculated radiation efficiency and effective gain are introduced with regard to the considerations mentioned above. Section V is concerned with investigations into the power absorbed in a head, a hand, and a shoulder on the power loss due to impedance mismatch and on the dissipated power in a nonexcited element when the whip length and the head-to-radio separation are changed. Mechanisms for the effective gain variations with respect to antenna structure and incident wave parameters will also be considered in Section V. From these results, a mechanism for obtaining a high radiation efficiency and a high effective gain is explained. In Section VI, the analytical results of the effective gain are verified by an experiment conducted in an indoor radiowave propagation environment.

II. Theoretical Model and Method

A. Antenna and Human Body Modeling

An external view of the diversity antenna model, which simulates a commercial hand-held terminal, is shown in Fig. 1(a). A metal cube represents the equipment body case. A whip antenna of length Lw is mounted at the top of the metal case, and a PIFA is attached on the side plate adjacent to the upper plate. It is known that a PIFA resonates when the element perimeter is a half-wavelength [12]. In Fig. 1(a), the dimensions of the element give a resonant frequency of nearly 900 MHz. A feed point of the PIFA, labeled "fp" in Fig. 1(a), is located at a position so that a good matching condition is obtained at 900 MHz.

Fig. 1(b) shows a model of a human phantom used for numerical calculations. Fig. 1(c) and (d) show the side view and front view of the human phantom. This represents a practical use condition with a simplified structure assuming biological human tissue parameters. The head is approximated by a circular

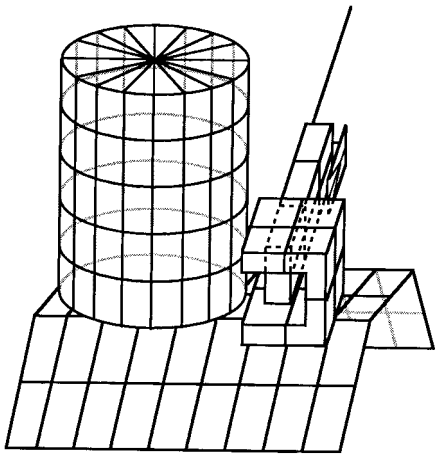

Fig. 2. Wire-grid model.

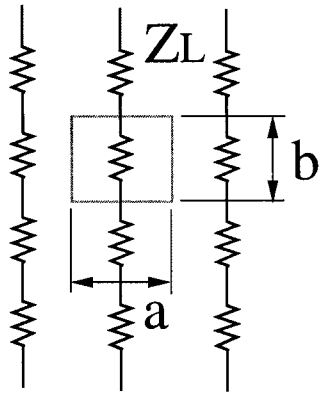

Fig. 3. Arrangement of the load impedances.

cylinder, the dimensions of which are 18 cm in diameter and 25 cm in height. The hand is modeled by a simple parallelepiped holding a model of a radio with a thickness of the palm of 2 cm. The distance between the lower edge of the PIFA and the upper edge of the hand is set to be 0.5 cm. The radio is placed inclined at angle α from the vertical and at distance D from the head so that it is positioned between the operator's mouth and ear. The rotation center of the radio is located at a distance of 2 cm from the top of the metal case and accords with the ear, which is located at a height of 12.5 cm from the surface of the shoulder, corresponding to the rotation center of the head, as shown in Fig. 1(c).

In previous studies, human phantoms consisting of only a head and a hand were used, and shoulder effects were not taken into account. In this work, we have attempted to simulate typical conditions in which a trapezoidal left shoulder is located at the side of a head giving a more realistic geometrical relationship between the human body and the radio during ordinary use. The dimensions and structure of the phantom shown in Fig. 1(b) are those of the average of 20- to 30-year-old men.

The wire-grid method illustrated in Fig. 2 was employed to calculate the antenna characteristics. The wire-grid model for a hand-held terminal is described in detail in the literature [1], [3], [24]. As shown in Fig. 2, the head consists of six circles and 16 straight lines, and the shoulder is divided by lines into a bent plane mesh structure. The validity of this structure will be verified by the measurements in Section III. A human body can be treated as a lossy dielectric material with the surface impedance calculated from the biological parameters of human tissue as

$$Z_S = \sqrt{\frac{j\omega\mu}{\sigma + j\omega\varepsilon}} \tag{1}$$

where

ε and μ	electric permittivity and the magnetic permeability;
σ	conductivity;
$\omega = 2\pi_f$ and f	frequency.

In order to simulate the human body by the wire-grid method, lumped load impedances are added into the wires as shown in Fig. 3 so that diagonal elements in the impedance matrix are modified to include the load impedance, which is related to the surface impedance by the following equation [6]:

$$Z_L = Z_S \frac{b}{a} \tag{2}$$

where a and b are the side lengths of the area in which the load impedance is located, as shown in Fig. 3.

B. Radiation Efficiency

In general, the input impedance of antennas positioned in free space is designed to be 50 Ω. Therefore, there would be an impedance mismatch loss when a hand-held terminal is located close to a human body because the input impedance of the antennas may change from that in free space. For this reason, the impedance mismatch loss must be considered in calculating the radiation efficiency. Since the two antennas are positioned close together, as shown in Fig. 1(a), the power radiated from the one is dissipated in the other. This condition would reduce the radiation efficiency and thus must be taken into account in the efficiency calculation.

The equivalent circuit at the feed points of the diversity antenna with one antenna excited and acting as a transmitter is represented in Fig. 4. Z_{11} and Z_{22} are, respectively, the self-impedances of the whip antenna and the PIFA, and Z_m is the mutual impedance. Z_{L1} and Z_{L2} are the load impedances seen from the antenna terminals into the RF circuit. Thus the antenna terminal voltages and currents are related by the following impedance matrix:

$$\begin{bmatrix} V_1 \\ V_2 \end{bmatrix} = \begin{bmatrix} Z_{11} & Z_m \\ Z_m & Z_{22} \end{bmatrix} \begin{bmatrix} I_1 \\ I_2 \end{bmatrix} \quad V_1 = -Z_{L1} I_1$$
$$V_2 = -Z_{L2} I_2. \tag{3}$$

If the load impedances Z_{L1}, Z_{L2} and the input impedances Z_{in1}, Z_{in2} are in the conjugate-matched condition, from (3) we obtain the following:

$$Z_{\text{in1}} = \frac{V_1}{I_1} = Z_{11} - \frac{Z_m^2}{Z_{L2} + Z_{22}}$$
$$Z_{\text{in2}} = \frac{V_2}{I_2} = Z_{22} - \frac{Z_m^2}{Z_{L1} + Z_{11}} \tag{4}$$
$$Z_{\text{in1}} = Z_{L1}^* \quad Z_{\text{in2}} = Z_{L2}^* \tag{5}$$

where the asterisk $(^*)$ denotes the complex conjugate. With a hand-held terminal placed in free space, the matched load im-

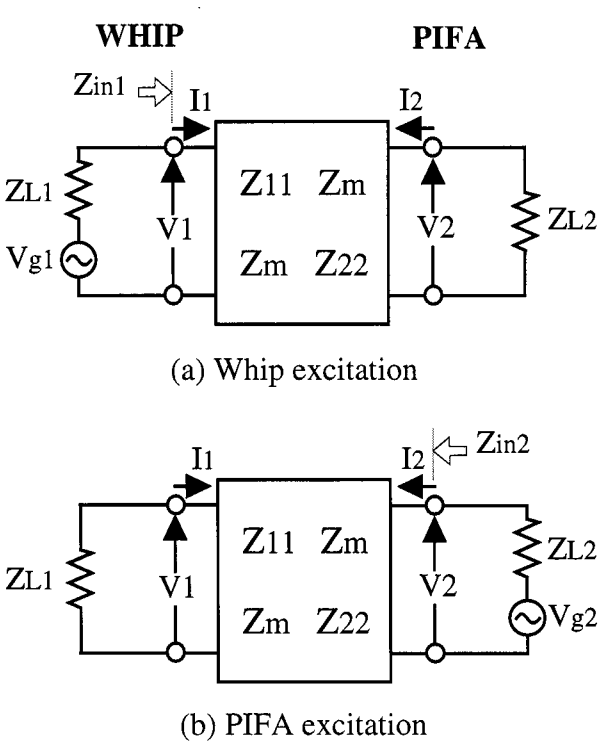

Fig. 4. Equivalent circuit of the diversity antenna.

pedances (Z_{L1m}, Z_{L2m}) satisfying (4) and (5) are assumed to be connected to the terminals of the two antennas. When the hand-held terminal approaches a human body, the self- and mutual-impedances are changed to be Z'_{11}, Z'_{22}, and Z'_m, and the input impedances become $Z'_{\rm in1}$ and $Z'_{\rm in2}$. Now we consider the case where the whip antenna is excited with voltage V_{g1}, as shown in Fig. 4(a). The input power $P_{\rm in}$ applied to the whip antenna is expressed by the following equation:

$$P_{\rm in} = \tfrac{1}{2}\,{\rm Re}[Z'_{\rm in1} I_1 I_1^*] \tag{6}$$

where

$$I_1 = \frac{V_{g1}}{Z_{L1m} + Z'_{\rm in1}}.$$

This power is transferred from generator 1 and is given from (6) as follows:

$$P_{\rm in} = \frac{1}{2}\frac{|V_{g1}|^2 {\rm Re}(Z'_{\rm in1})}{|Z_{L1m} + Z'_{\rm in1}|^2} = P_{\rm av} \cdot S \tag{7}$$

where

$$P_{\rm av} = \frac{|V_{g1}|^2}{8{\rm Re}(Z_{L1m})}$$

and

$$S = \frac{4{\rm Re}(Z_{L1m}){\rm Re}(Z'_{\rm in1})}{|Z_{L1m} + Z'_{\rm in1}|^2} \le 1.$$

${\rm Re}[X]$ represents the real part of X and $P_{\rm av}$ denotes the available power from the generator. S expresses the ratio of power delivered to the antenna to power available from the generator, which is unity under the conjugate-matched condition. Let us

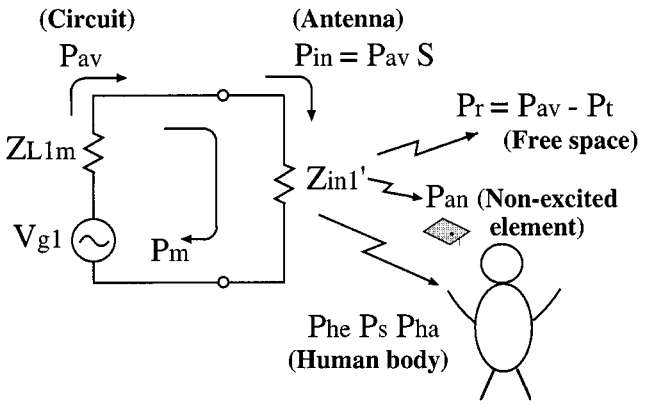

Fig. 5. Relationship between the dissipated powers (whip excitation).

define radiation efficiency η with respect to the available power using the following relationship:

$$\eta = \frac{P_r}{P_{\rm av}} = \frac{P_{\rm av} - P_t}{P_{\rm av}} \quad P_t = P_{\rm he} + P_{\rm ha} + P_s + P_{\rm an} + P_m \tag{8}$$

where

P_r	power radiated into the air;
P_t	total power loss;
$P_{\rm he}$, $P_{\rm ha}$ and P_s	powers absorbed in the head, the hand, and the shoulder, respectively.

$P_{\rm an}$ is the power dissipated in the matched load Z_{L2m} of the PIFA and P_m is the power loss due to the impedance mismatch. The relationship of these powers is illustrated schematically in Fig. 5, and they can be calculated from the following equations:

$$P_{\rm he} = \tfrac{1}{2}\sum {\rm Re}(Z_{\rm Lhe}) I_{\rm he}^2 \tag{9}$$

$$P_{\rm ha} = \tfrac{1}{2}\sum {\rm Re}(Z_{\rm Lha}) I_{\rm ha}^2 \tag{10}$$

$$P_s = \tfrac{1}{2}\sum {\rm Re}(Z_{\rm Ls}) I_s^2 \tag{11}$$

$$P_{\rm an} = \tfrac{1}{2}{\rm Re}[Z_{L2m} I_2 I_2^*] \tag{12}$$

$$P_m = (1 - S) P_{\rm av} \tag{13}$$

where $Z_{\rm Lhe}$, $Z_{\rm Lha}$, and $Z_{\rm Ls}$ are the load impedances in the head, the hand, and the shoulder, respectively; and $I_{\rm he}$, $I_{\rm ha}$, and I_s are the currents through each load. Usually, radiation efficiency is defined as the ratio of total radiated power to the net power accepted by the antenna $P_r/P_{\rm in}$ [13]. Our definition in (8) is a measure of how effectively the antenna converts available power $P_{\rm av}$ into transmitted power P_r. This radiation efficiency is analogous to transducer power gain in the design of two-port networks (e.g., amplifiers) in circuit theory [14] and is useful in considering the general case, since it includes the effect of impedance mismatch P_m. In the same way, where the PIFA is excited, the radiation efficiency can be obtained from Fig. 4(b) and (8).

C. Mean Effective Gain

When an antenna moves in a multipath propagation environment over a random route, the mean effective gain (MEG) is obtained using the following equation [2]:

$$G_e = \frac{P_{\rm rec}}{P_1 + P_2}. \tag{14}$$

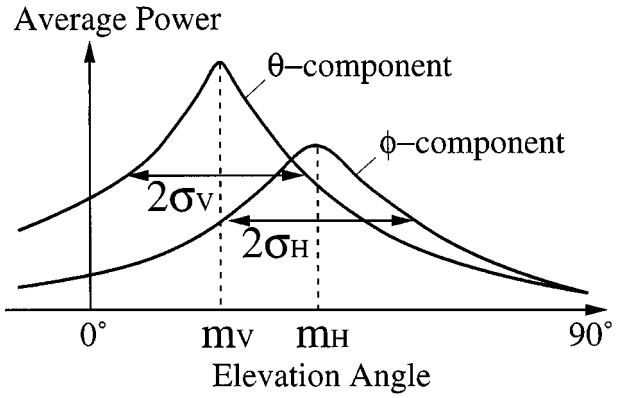

Fig. 6. Incident wave model.

$P_{\rm rec}$ is the mean received power of an antenna over the random route, P_1 is the mean power received by a θ-polarized isotropic antenna in a mobile radio environment, and P_2 is the mean power received by a ϕ-polarized isotropic antenna. Thus, $P_1 + P_2$ is the total mean incident power of an antenna averaged over the route. $P_{\rm rec}$ is expressed by Yeh as follows [15]:

$$P_{\rm rec} = \int_0^{2\pi} \int_0^{\pi} \{P_1 G_\theta(\Omega) P_\theta(\Omega) + P_2 G_\phi(\Omega) P_\phi(\Omega)\}\, d\Omega \tag{15}$$

where Ω denotes components (θ, ϕ) in spherical coordinates and $d\Omega = \sin\theta d\theta d\phi$. $G_\theta(\Omega)$ and $G_\phi(\Omega)$ are the θ and ϕ components of the antenna power gain pattern, which take account of the impedance mismatch loss, and $P_\theta(\Omega)$ and $P_\phi(\Omega)$ are the θ and ϕ components of the angular density functions of incoming plane waves. Since the mean incident power ratio P_1/P_2 represents the cross-polarization power ratio (XPR)

$$\text{XPR} = \frac{P_1}{P_2} \tag{16}$$

the expression for the MEG can be represented by the following equation derived from (14)–(16):

$$G_e = \int_0^{2\pi} \int_0^{\pi} \left[\frac{\text{XPR}}{1+\text{XPR}} G_\theta(\Omega) P_\theta(\Omega) + \frac{1}{1+\text{XPR}} G_\phi(\Omega) P_\phi(\Omega) \right] d\Omega. \tag{17}$$

$P_\theta(\Omega)$ and $P_\phi(\Omega)$ are from a statistical model in which the angular density functions are assumed to be Gaussian in elevation and uniform in azimuth as shown in Fig. 6, and are given by

$$P_\theta(\theta, \phi) = A_\theta \exp\left[-\frac{\left\{\theta - \left(\frac{\pi}{2} - m_v\right)\right\}^2}{2\sigma_v^2} \right] \quad (0 \le \theta \le \pi) \tag{18}$$

$$P_\phi(\theta, \phi) = A_\phi \exp\left[-\frac{\left\{\theta - \left(\frac{\pi}{2} - m_H\right)\right\}^2}{2\sigma_H^2} \right] \quad (0 \le \theta \le \pi) \tag{19}$$

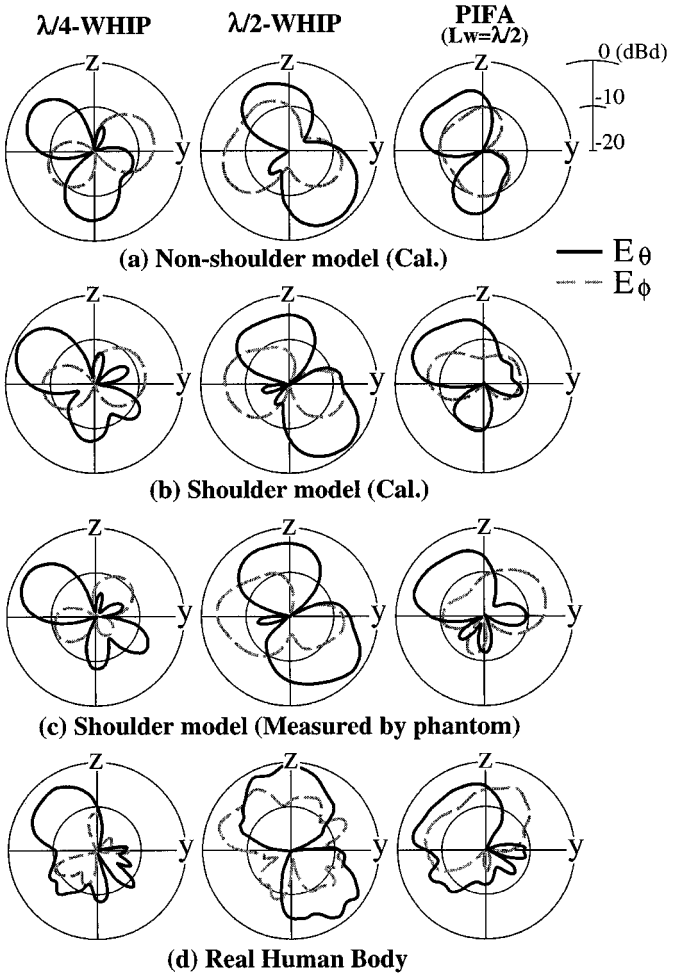

Fig. 7. Radiation pattern calculated by (a) the nonshoulder model and (b) the shoulder model, and radiation pattern measured by (c) the human phantom shoulder model and (d) a real human body at $\alpha = 60°$ and $D = 2$ cm.

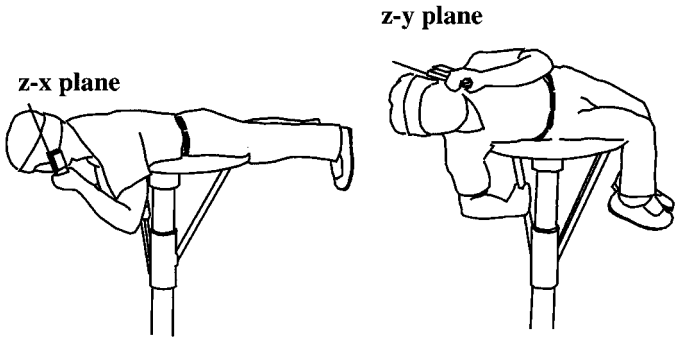

Fig. 8. Measurement method for the radiation pattern in the vertical plane ($z - x$ and $z - y$).

where m_V and m_H are the mean elevation angles of the θ- and ϕ-component wave distributions observed from the horizontal direction. σ_V and σ_H are the standard deviations of the θ- and ϕ-component wave distributions. A_θ and A_ϕ are proportional constants determined by the following equation:

$$\int_0^{2\pi} \int_0^{\pi} P_\theta(\Omega)\, d\Omega = \int_0^{2\pi} \int_0^{\pi} P_\phi(\Omega)\, d\Omega = 1. \tag{20}$$

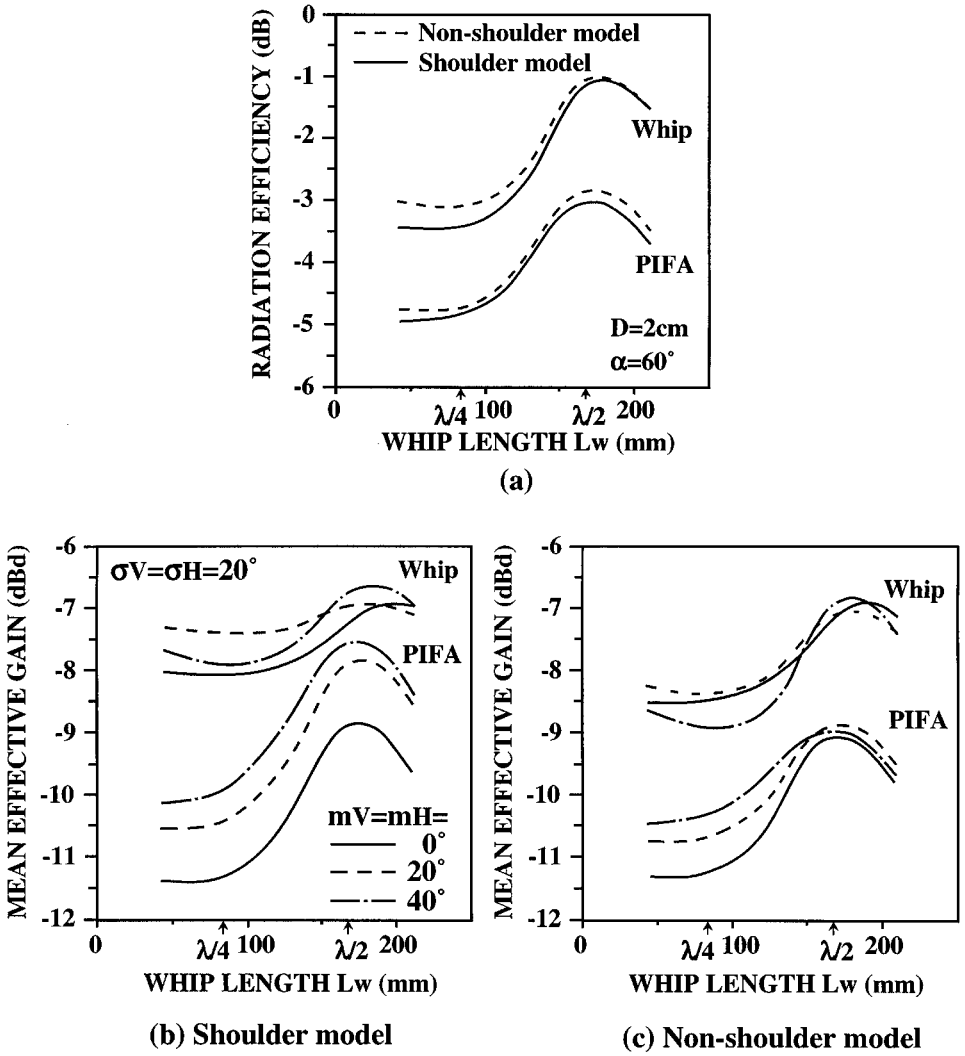

Fig. 9. (a) Radiation efficiency and (b), (c) MEG calculated by the shoulder and nonshoulder models at $\alpha = 60°$ and $D = 2$ cm.

III. Effect of the Shoulder on Effective Gain Characteristics

A. Radiation Characteristics

Incident radiowaves coming from a base station are known to be distributed in the elevation angle between 0–40° in a land mobile communication environment in the 900-MHz band [16]. Therefore, for accurate evaluation of portable telephone antennas, it is essential to obtain accurate radiation patterns at those angles of signal arrival. Thus, in this section, the influence of the shoulder on the radiation characteristics at the high elevation angles is examined by comparing the characteristics for the human model with the shoulder, shown in Fig. 1, with those without the shoulder corresponding to the cylindrical head and parallelepiped hand only in Fig. 1. These are referred to as "the shoulder model" and "the nonshoulder model," respectively.

Fig. 7(a) and (b) shows the radiation patterns in the vertical plane ($z - y$) calculated for the shoulder and nonshoulder models. The frequency was 900 MHz, and the whip antenna was of a quarter-wavelength (83 mm) or a half-wavelength (167 mm). Fig. 7(a) and (b) shows the different radiation properties of the two antennas. For a $\lambda/4$-whip antenna, the radiation in the lower hemispherical (negative-z) region toward the shoulder is suppressed in the case of the shoulder model and consequently the dominant radiation occurs in the upper hemispherical (positive-z) region toward the sky.

In contrast, for a $\lambda/2$-whip antenna, there is a strong radiation in the lower hemispherical region toward the shoulder, and little change is observed between the shoulder and nonshoulder models. It is clear from Fig. 7(a) and (b) that gain enhancement due to the shoulder in the high elevation angles occurs in the case of a shorter whip antenna. This effect can be deduced from the fact that the distance between the maximum point of the current distribution on whip antennas and the phantom shoulder differs for the two whip antennas (see Figs. 1 and 17), and for a shorter whip antenna, the shoulder functions as a reflector, since the shoulder is spread over as a conformal plane at a distance of a quarter- to half-wavelength from the antenna. Fig. 7(a) and (b) indicates that this explanation is also true for the PIFA, in which the radiation occurs just above the shoulder, and thus the radiation to the negative-z direction is suppressed due to the shoulder.

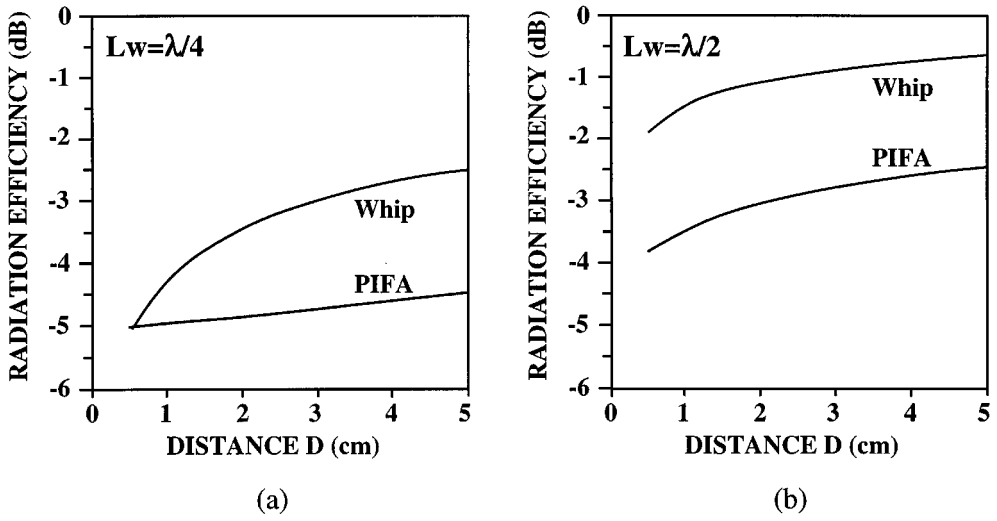

Fig. 10. Radiation efficiency versus the distance between the human head and the radio body at $\alpha = 60°$: (a) $Lw = \lambda/4$ and (b) $Lw = \lambda/2$.

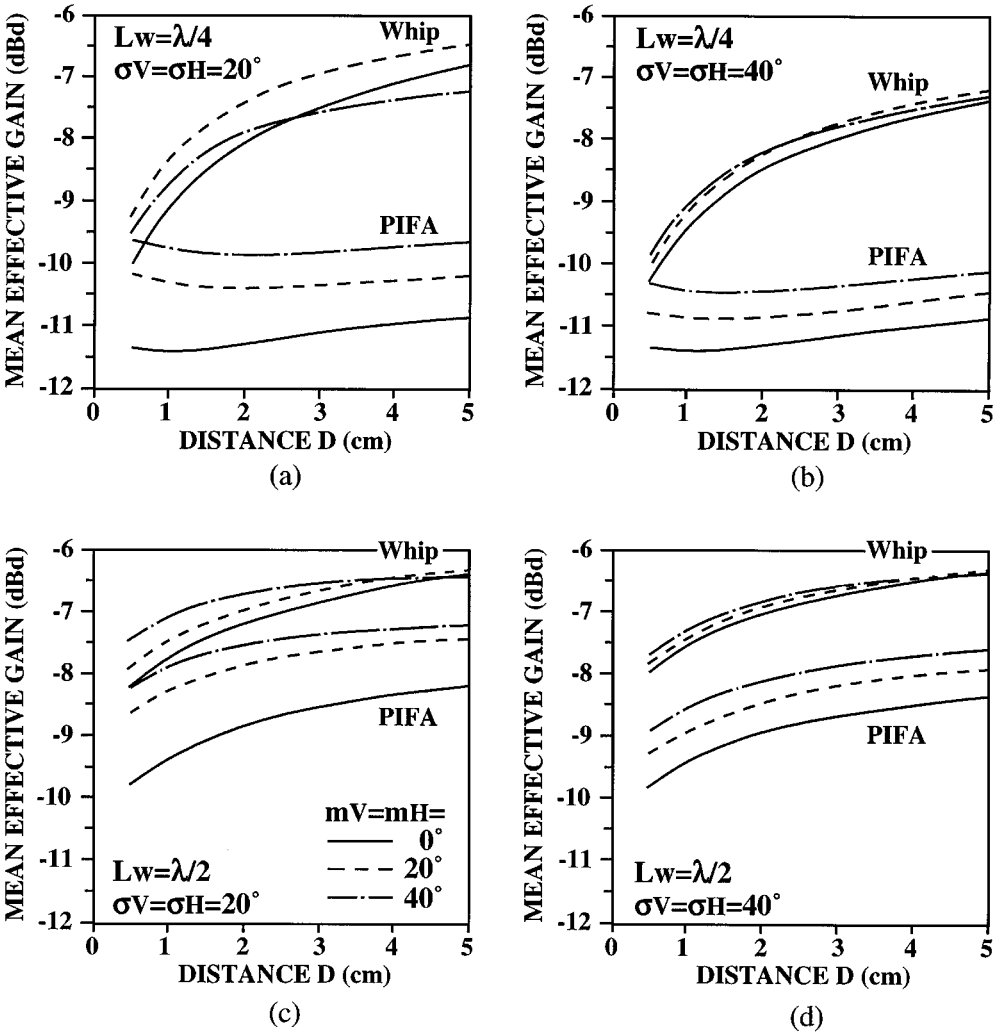

Fig. 11. Mean effective gain versus the distance between the human head and the radio body at $\alpha = 60°$ and XPR = 6 dB: (a) $Lw = \lambda/4, \sigma V = \sigma H = 20°$; (b) $Lw = \lambda/4, \sigma V = \sigma H = 40°$; (c) $Lw = \lambda/2, \sigma V = \sigma H = 20°$; and (d) $Lw = \lambda/2, \sigma V = \sigma H = 40°$.

Fig. 7(c) shows the measured results of a human phantom. The phantom has the same shape as the human model in Fig. 1 and is made of polypropylene plastic of 3-mm thickness. A mixed solution comprising 0.6 N salt and ethyleneglycol normal

solutions, with a weight ratio of 35:65 with a relative permittivity of 45 and a conductivity of 0.9 S/m [17], is contained in the phantom plastic case. A small oscillator device was installed inside the radio case in order to eliminate the influence of coaxial cable. Comparing Fig. 7(b) and (c), the calculated radiation pattern of the shoulder model shows good agreement with the measured radiation pattern of the human phantom, indicating the validity of the wire-grid modeling in Fig. 2.

Fig. 7(d) shows the measured radiation pattern for a 30-year-old man of 170 cm height and 60 kg weight. The measurement was made by laying the man on a rotation table, while holding the radio terminal in Fig. 1(a) next to the ear with an inclination angle of 60°, as shown in Fig. 8 [18]. The rotation table is made of a plastic plate with a diameter of 70 cm. In the measurement, the lower part of the conductive radio body was covered with a styrene foam plate of 1-cm thickness for insulation. Comparing Fig. 7(d) and (b) or (c), there are slight differences between the two radiation patterns in the lower hemispherical region. This is probably due to a simple approximation of the human phantom model. However, Fig. 7(d) shows the radiation characteristics such that the radiation to the shoulder direction is suppressed and the radiation to the high elevation angles is enhanced. In addition, the radiation patterns in Fig. 7(d) agree very well with the results in Fig. 7(b) and (c) in the upper hemispherical region toward the sky. From this, the human model is found to be reasonably accurate in evaluating practical radiation characteristics at elevation angles typical of mobile radio signal arrival.

B. Effective Gain Characteristics

In this section, we investigate how the change in the radiation characteristics due to the existence of the shoulder affects the effective gain in a multiple radiowave environment, and the condition under which the shoulder is necessary for modeling the human body is considered.

Fig. 9 exhibits the calculated radiation efficiency and MEG as a function of the whip length Lw. Fig. 9 (b) and (c) shows the MEG for the shoulder and nonshoulder models. The incident radiowave parameters are determined to be typical values in urban areas; the XPR is 6 dB, the mean elevation angles are 0° to 40°, and the standard deviation is 20°. The detailed explanations and considerations concerning the relationship between these radiowave parameters and the antenna characteristics are given in the next section. In this section, we focus on the effect of the shoulder.

Comparing the radiation efficiency of the shoulder and nonshoulder models in Fig. 9(a), a reduction in efficiency is observed in the case of the shoulder model for both antennas. This is caused by the power absorbed in the shoulder, which will be discussed in Section V. In contrast, comparing Fig. 9(b) and (c), a relatively large increase in the MEG due to the existence of the shoulder can be seen for a λ/4-whip antenna and a PIFA with $Lw = \lambda/2$, but the increment is very small for a λ/2-whip antenna and a PIFA with $Lw = \lambda/4$. It should be noted that the higher the elevation angle of incident waves, the larger the increment in the MEG. For example, for a $\lambda/4$-whip antenna, the increment in the MEG is 0.4, 1, and 1 dB for $m_V = m_H = 0°$, 20°, and 40°, respectively. For a PIFA with $Lw = \lambda/2$, the increment is 0.3, 1.1, and 1.5 dB for $m_V = m_H = 0°$, 20°, and 40°, respectively. This MEG enhancement is caused by the radiation pattern change in the direction of incident waves, as shown in Fig. 7. These facts suggest that the existence of the shoulder should be taken into account when an adequately accurate evaluation of the radiation characteristics of portable telephone antennas is needed, especially for a short whip antenna and a built-in PIFA in urban radiowave environments where the incident waves tend to arrive from the high elevation angles.

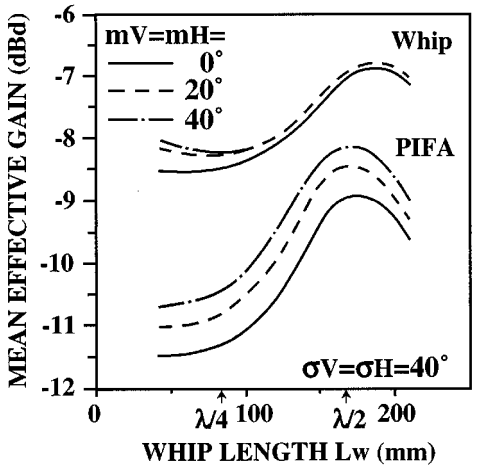

Fig. 12. Mean effective gain versus the whip length at $\alpha = 60°$, $D = 2$ cm, XPR = 6 dB, and $\sigma V = \sigma H = 40°$.

IV. Analytical Results

Fig. 10 shows the radiation efficiency as a function of head-to-radio separation D with a fixed radio inclination angle α of 60°. The frequency is 900 MHz, and the whip antenna is of a quarter-wavelength [Fig. 10(a)] and a half-wavelength [Fig. 10(b)]. The relative permittivity of human brain tissue used in the calculation is 42, and the conductivity is 0.85 S/m [19]. From Fig. 10(a), the radiation efficiency of the whip antenna increases significantly with increasing D, while that of the PIFA increases gradually. This effect can be interpreted in terms of the power absorbed in the head and hand. For the PIFA, the power absorbed in the hand is greater than that in the head, and the effect of the head becomes relatively small (see Section V in detail). As the radio approaches the head, a significant reduction in efficiency is seen, and consequently less than half of the available power is radiated into the air, which is consistent with previous studies [7], [8], [26], [9].

When $Lw = \lambda/2$, on the other hand, the efficiencies increase considerably for both antennas as in Fig. 10(b). This significant increase in efficiency is mainly caused by the reduction in power dissipated in the matched load $P_{\rm an}$ (see Fig. 16). Comparing Fig. 10(a) and (b), it can be seen that the increasing rate with D of the PIFA efficiency is changed from the $Lw = \lambda/4$ to the $Lw = \lambda/2$ case. This is attributed to the fact that when $Lw = \lambda/2$, the power absorbed in the head $P_{\rm he}$ for the PIFA increases compared with the $Lw = \lambda/4$ case, as shown in Fig. 16(b), and thus the efficiency of the PIFA for $Lw = \lambda/2$ increases more rapidly than that for $Lw = \lambda/4$, since $P_{\rm he}$ reduces with increasing D.

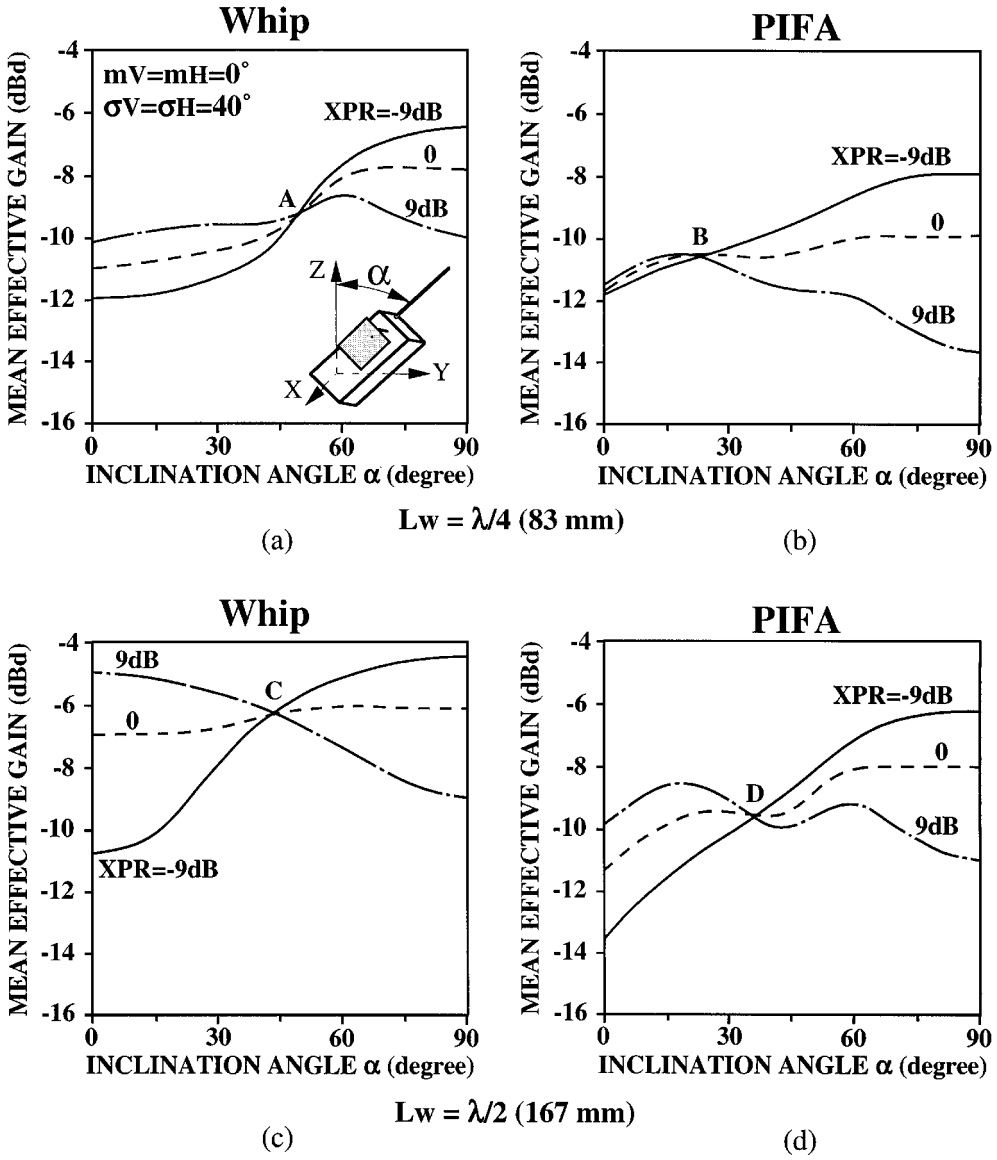

Fig. 13. Mean effective gain versus the inclination angle of the radio body at $D = 2$ cm: (a), (b) $Lw = \lambda/4$ and (c), (d) $Lw = \lambda/2$.

Fig. 11 exhibits the MEG with respect to D with whip length, elevation angle, and standard deviation of the incident waves as parameters. It is known that the incident waves in the 900-MHz land mobile environment arrive from elevation angles of 0–40° in urban areas with the waves spread over a wide angle, and thus the mean elevation angles m_V and m_H are assumed to be 0–40°, and the standard deviations σ_V and σ_H are assumed to be between 20–40°.

From Fig. 11(a) and (b), it can be seen that when $Lw = \lambda/4$, the MEG for the whip antenna decreases as the hand-held terminal approaches the head. For instance, Fig. 11(a) shows that when $D = 2$ cm, which may be the normal separation in practical use, the MEG for the whip antenna is -8.2 to -7.5 dBd for m_V and m_H from 0° to 20° and increases rapidly with increasing D, whereas the MEG for the PIFA becomes as low as -11.3 to -9.8 dBd for m_V and m_H from 0° to 40° and increases gradually with increasing D. This behavior is similar to that of the radiation efficiency, as shown in Fig. 10. From this, the variation in the MEG with changing the elevation angle from 0° to 40° is found to be 0.7 dB for the whip antenna and 1.5 dB for the PIFA at $D = 2$ cm. These values become smaller as the incident waves are spread over a wide angle, as shown in Fig. 11(b). It can be seen from these results that the PIFA is more influenced by the radiowave environment under the condition assumed in Fig. 11. The reason for this phenomenon will be dealt with in Section V.

When Lw becomes longer up to a half-wavelength as in Fig. 11(c) and (d), there is a significant increase in the MEG. For example, when $D = 2$ cm and $m_V = m_H = 0°$, the increment in the MEG for the whip antenna from $Lw = \lambda/4$ to $\lambda/2$ is 1 and 1.5 dB for standard deviations of 20° and 40°, respectively, and is 2.5 dB for the PIFA for both standard deviations. It is interesting to note that an increase in whip length brings about a more effective MEG enhancement of the PIFA. In addition, Fig. 11(c) and (d) shows that the increasing rate with D of the MEG is changed from $Lw = \lambda/4$ to $\lambda/2$

for the PIFA. The results are similar to those of the radiation efficiency in Fig. 10.

It should be noted from Fig. 11 that the MEG performance is strongly dependent on the type of antenna used, which arises from a different electromagnetic interaction between the antenna and a human operator. The mechanism for this complicated problem will be dealt with in the next section.

Fig. 12 shows the MEG with respect to the whip length Lw for XPR = 6 dB and $\sigma_V = \sigma_H = 40°$. Fig. 9(b) shows the MEG for $\sigma_V = \sigma_H = 20°$, and the solid curves in Fig. 9(a) show the radiation efficiency which are companion data for Fig. 12. In the figures, the radiation efficiencies and the MEG change depending on Lw, and there is an optimum whip length for obtaining high efficiency and MEG. The optimum whip lengths are near $Lw = \lambda/2$ for both antennas.

Figs. 9(b) and 12 also show that the variation in the MEG of the whip antenna is small with changing whip length, while that of the PIFA is large. Of particular interest is that, as Lw becomes longer, the increment in the MEG of the whip antenna in Figs. 9(b) and 12 is smaller than that in efficiency in Fig. 9(a), while the increment in the MEG of the PIFA almost agrees with that in efficiency. The reason for this behavior will be discussed in Section V.

Figs. 9(b) and 12 also show that the variation in the MEG of the whip antenna is small with changing elevation angles of the incident waves, while that of the PIFA is large, which are similar to the results in Fig. 11. On the other hand, the MEG of a vertically oriented whip antenna without a human body (in [4, Fig. 4, p. 900], [25]) varies considerably as the values of m_V and m_H change, while that of the PIFA does not. The reason for this behavior will also be discussed in Section V.

Fig. 13 exhibits the MEG as a function of radio body inclination angle from the vertical with XPR as a parameter. The whip is of a quarter-wavelength or a half-wavelength, which is a basic antenna configuration from the design viewpoint. It is noted from the figure that there are particular inclination angles at which the MEG becomes constant regardless of the value of XPR. These inclination angles are labeled A, B, C, and D in Fig. 13, and they are at 47°, 23°, 43°, and 35°, respectively. Also, at certain XPR values, the variation in the MEG is small regardless of the antenna inclination angle. For instance, when XPR = 0 dB, the MEG of the $\lambda/2$ whip antenna is nearly constant at -6 dBd. It is reported that the XPR depends very much on the propagation environment [20] and ranges from 0 to 9 dB. From Fig. 13, we can estimate the change in the MEG with changing XPR in a practical situation where the average inclination angle is about 60° [21]. For instance, in the case of $Lw = \lambda/4$, the changes in the MEG for the whip antenna and PIFA are estimated to be 0.8 and 2 dB, respectively, with a variation of XPR from 0 to 9 dB.

V. Considerations

A. Power Loss and Current Distribution

In order to consider the radiation efficiency behavior described in Section IV, the power losses caused by the absorption of each region of the human body ($P_{\rm he}$, $P_{\rm ha}$, and P_s) and by a hand-held terminal itself ($P_{\rm an}$ and P_m) were investigated.

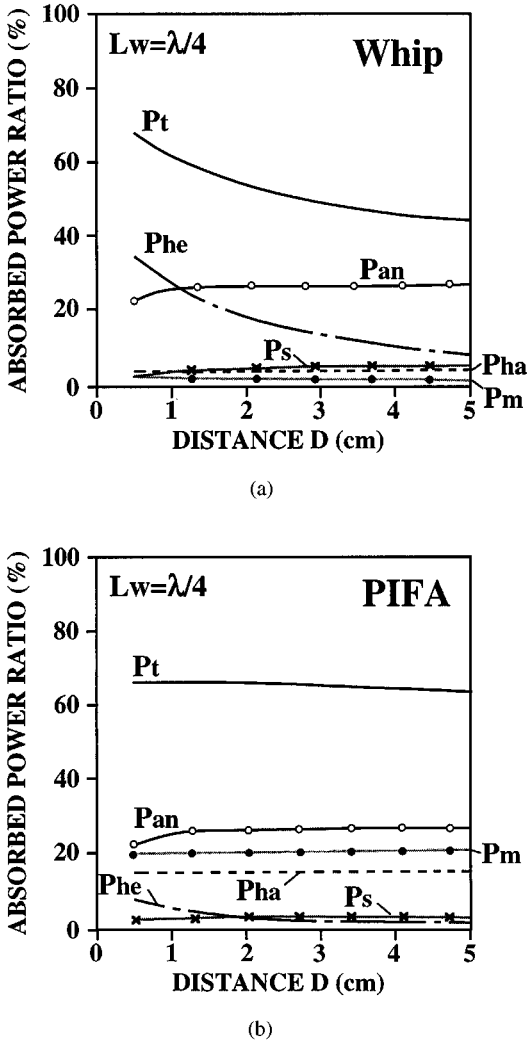

Fig. 14. Dissipated power versus the distance between the human head and the radio body at $\alpha = 60°$: (a) whip and (b) PIFA.

Fig. 14(a) and (b) shows the results calculated as a function of head-to-radio separation D with $Lw = \lambda/4$ and $\alpha = 60°$. In each case, the power is normalized to the available power $P_{\rm av}$. Concerning the whip antenna, $P_{\rm he}$ decreases as D increases, and this leads to a reduction of the total power loss P_t. Fig. 14(a) also shows that $P_{\rm he}$ and $P_{\rm an}$ for the whip antenna are the major contributory factors to P_t when D is small. In the case of the PIFA, however, P_m, $P_{\rm ha}$, and $P_{\rm an}$ are the major factors, and they are almost constant regardless of D. To investigate this phenomenon, the impedances for both antennas are calculated and measured.

Fig. 15 illustrates the calculated impedance characteristics of the whip antenna and the PIFA as a function of head-to-radio distance, together with the impedances measured by the human phantom described in Section III and the real human body of a 30-year-old man. The whip antenna is of a quarter-wavelength, and load impedances (Z_{L1} and Z_{L2} in Fig. 4) of 50 Ω are connected to both terminals. In the figure, dashed lines indicate the impedances of the antennas in free space. From Fig. 15, the impedances of the whip antenna change appreciably as D changes, while those of the PIFA remain almost constant regardless of the

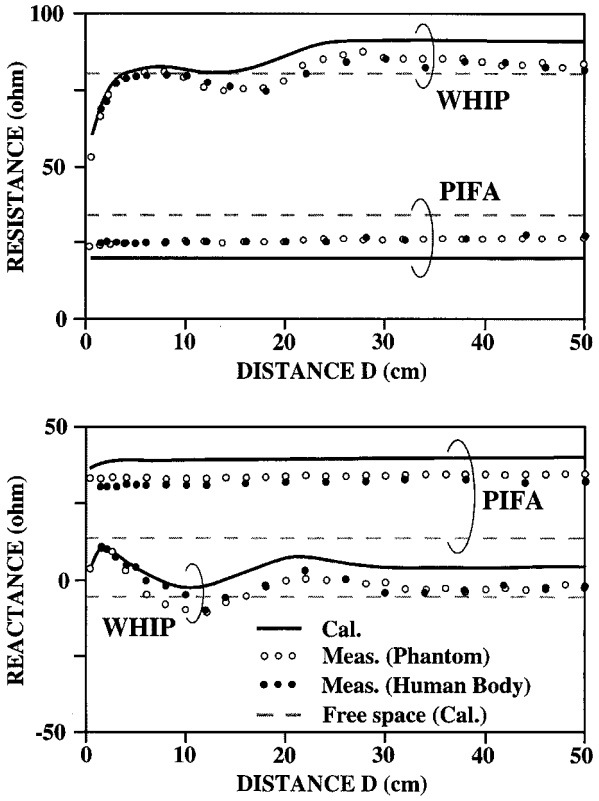

Fig. 15. Impedance versus radio-to-head distance at $\alpha = 60°$.

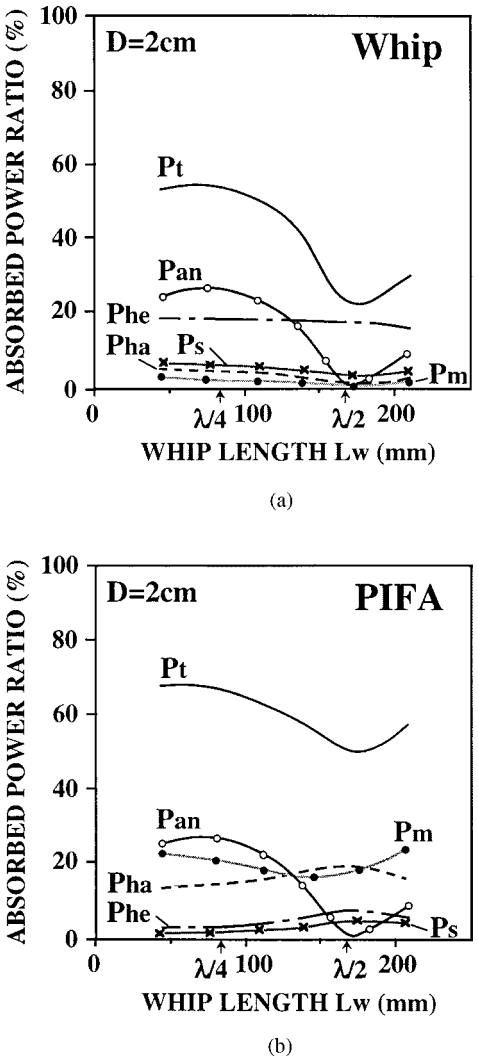

Fig. 16. Dissipated power versus whip length at $\alpha = 60°$ and $D = 2$ cm: (a) whip and (b) PIFA.

distance. In addition, the figure shows that greater variations in impedance from the free space impedance are observed in the case of the PIFA compared to the whip antenna case. The larger power loss due to impedance mismatch for the PIFA shown in Fig. 14(b) can be interpreted in terms of this greater variation in impedance from the free space impedance.

Fig. 16(a) and (b) shows the power losses with respect to whip length Lw. $P_{\rm an}$ decreases with increasing Lw, and the minimum value of 0% is obtained when $Lw = \lambda/2$. This behavior gives a minimum value of P_t at the same value of Lw, corresponding to the radiation efficiency shown by solid lines in Fig. 9(a). Reduction in $P_{\rm an}$ is related to the current induced on the nonexcited element. Fig. 17 shows the current distribution with a whip antenna excited with a voltage of 1 V for $D = 2$ cm and $\alpha = 60°$. It is found from Fig. 17 (a) and (b) that when the whip antenna is of a quarter-wavelength, a large current flow is induced on the PIFA, whereas the current is very small in the case of a half-wavelength whip antenna. This suggests that in these cases, the changes in $P_{\rm an}$ can be accounted for by changes in the currents induced on the PIFA.

Fig. 16(a) also shows that a decrease in absorbed power in the hand $P_{\rm ha}$ is seen near $Lw = \lambda/2$ in the case of the whip antenna. This effect can be explained in terms of a smaller current flow on the conducting radio case when $Lw = \lambda/2$, leading to a small current induced on the hand, as shown in Fig. 17. On the other hand, Fig. 16(b) shows that increases in the absorbed powers ($P_{\rm he}$, $P_{\rm ha}$, P_s) are observed near $Lw = \lambda/2$ in the case of the PIFA. This phenomenon is interpreted by the fact that an increase in Lw leads to a greater radiated power into the air due to a decrease in $P_{\rm an}$ and P_m, thus resulting in an increase in the absorbed powers ($P_{\rm he}$, $P_{\rm ha}$, P_s) in the human body, since the shape of the radiation patterns of the PIFA does not change appreciably with changing whip length, as shown in Fig. 18.

B. Radiation Patterns

As described in Section IV, when a portable telephone is in an inclined configuration, the mean effective gains of the whip antenna and the PIFA change considerably as the whip length changes. The reason for this phenomenon was considered by calculating changes in the radiation patterns of both antennas since the MEG mainly depends on the radiation patterns rather than antenna efficiency. Fig. 18 shows the radiation patterns in the vertical plane ($z - y$) of the whip antenna and the PIFA with respect to whip length from $\lambda/8$ to $5/8\lambda$. The frequency is 900 MHz. As can be seen from the figure, the whip antenna shows little change in radiation intensity in the upper hemispherical region particularly for whip lengths between $\lambda/8$ and $3/8\lambda$ [Fig. 18(a)–(c)]. This is the reason for little variation in the MEG of the whip antenna for whip lengths of $\lambda/8$ to $3/8\lambda$ in

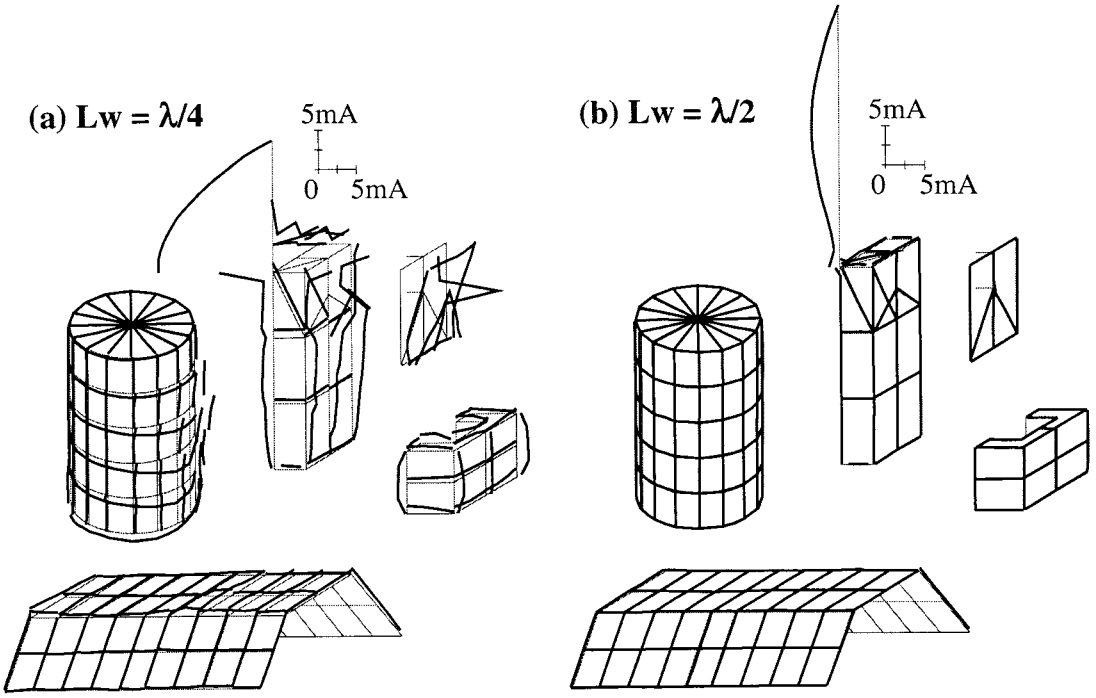

Fig. 17. Current distribution versus whip length at $\alpha = 60°$ and $D = 2$ cm with whip excitation of $V_1 = 1$ V: (a) $Lw = \lambda/4$ and (b) $Lw = \lambda/2$.

Figs. 9(b) and 12. In contrast, in Fig. 18, the PIFA offers a significant change in radiation intensity at elevation angles of 0° to 40°, which are the average directions of signal arrival from a base station. For example, at an elevation angle of 20°, the increase in radiation intensity is as large as 8 dB as the whip length increases from $\lambda/8$ to $\lambda/2$. These radiation pattern changes explain the large MEG changes of the PIFA with respect to whip length in Figs. 9(b) and 12.

As mentioned in Section III, in the case of the whip antenna, as Lw becomes longer, the stronger radiation occurs in the lower hemispherical region toward the shoulder, which is clearly demonstrated in Fig. 18(c)–(e). However, this radiation is very small in the case of the PIFA. This explains why as Lw becomes longer, an increment in the MEG of the whip antenna in Figs. 9(b) and 12 is smaller than the increment in efficiency in Fig. 9(a), while the increment in the MEG of the PIFA is almost the same as the increment in efficiency.

Figs. 11(a) and 9(b) at $Lw = \lambda/4$ show that for the whip antenna, the MEG has a greater value when $m_V = m_H = 20°$, while for the PIFA, the MEG has a greater value when $m_V = m_H = 40°$. This phenomenon can be explained from the fact that the maximum radiation direction exists near 20° for the whip antenna and 40° for the PIFA when $Lw = \lambda/4$, as in Fig. 18(b).

It is found from Figs. 11(a) and (c) and 9(b) that variations in the MEG of the whip antenna are small with changing elevation angles of the incident waves, while those of the PIFA are large. In particular, the MEG of the PIFA at $m_V = m_H = 0°$ is significantly smaller than that at $m_V = m_H = 20°$ and 40°. The reason for this behavior is explained in terms of a deep null observed in the E_θ-radiation pattern of the PIFA at $\theta = 90°$ (horizontal direction) in Fig. 18. However, as the standard deviations are large, as in Figs. 11(b) and (d) and 12, the variations in the MEG with respect to the elevation angles become smaller since in such a situation, the radiation patterns at high elevation angles mainly determine the MEG values.

VI. Experimental Study in an Indoor Multipath Environment

In order to verify the validity of the analytical results in Section IV, an experiment was made in an indoor multiple radiowave environment to estimate the MEG characteristics at 900 MHz. Fig. 19 shows the experimental setup. The experimental procedure and method for incident wave parameter measurement for indoor environments have been reported by Taga [22]. The experiment was conducted in a typical laboratory with concrete walls and plastic boards on a concrete base for the floor and ceiling. The transmitting antenna was located vertically on the floor and the receiving signals were sampled by an analog-to-digital converter simultaneously with the receiving whip antenna and PIFA close to the human phantom (Fig. 1), which was moving around on a rotating arm of 1.5 m. A partition wall was placed between the transmitting and receiving antennas so that the out-of-sight condition was maintained. Both antennas were located at the same height of 1.5 m from the floor, which was the ceiling–floor center position. In this configuration, the incident waves are assumed to have a symmetrical distribution in elevation with the maximum value in the horizontal direction. If we assume the incident wave distribution to be Gaussian in elevation, then the incident wave can be represented by three parameters:

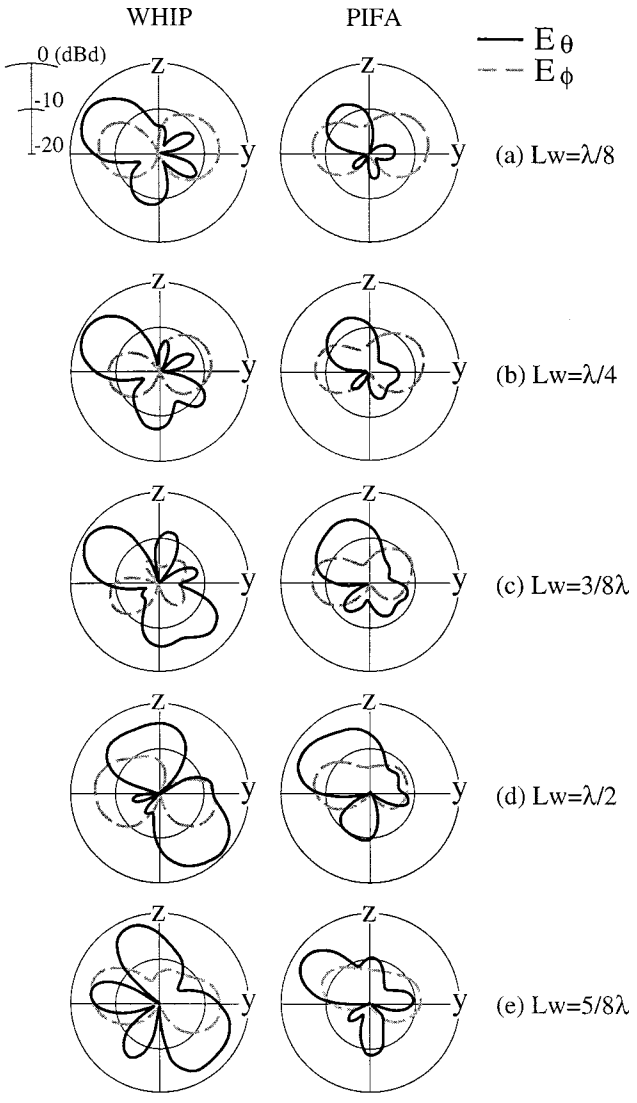

Fig. 18. Whip length versus radiation characteristics at $\alpha = 60°$ and $D = 2$ cm.

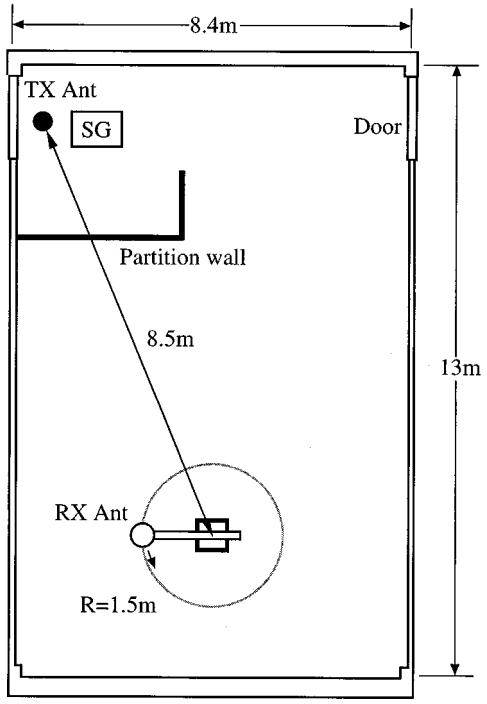

Fig. 19. Indoor experimental setup of multiple radio wave propagation.

TABLE I
MEASUREMENT RESULTS OF INCIDENT WAVE PARAMETERS

XPR	σ_V	σ_H
4.4dB	27°	58°

the XPR and the standard deviations of the vertically and horizontally polarized components σ_V and σ_H, respectively. XPR was measured by the ratio of the average receiving power of a half-wavelength dipole antenna to that of a cylindrical slot antenna when the two antennas rotate once. The slot antenna was 28 mm in cylinder diameter, 246 mm in slot length, and 1 mm in slot width, and was fed by a coaxial cable through a parallel matching capacitor of 2 pF. The slot antenna has an omnidirectional radiation pattern in azimuth and a figure-eight pattern in elevation with a dominant E_ϕ polarized component when the antenna is located vertically. The standard deviation can be found from the MEG characteristics for the dipole and slot antennas located vertically and horizontally. The total incident power required for the MEG calculation was measured by the dipole antenna skewed by 55° from the vertical. Since there may have been some deviation in the azimuthal angle of the incident waves, the MEG was calculated from an average of four successive measured results in which each measurement was made for the human phantom at four different angular positions at 90° intervals relative to the tangential direction of the rotating arm. The detailed measurement procedure is given in the literature [22].

Table I shows the measured incident wave parameters. The results indicate that the transmitted vertically polarized component is dominant. This phenomenon can be interpreted as being due to multiple radiowaves' being created by reflections from the walls, floor, and ceiling in a regular manner since there is no furniture such as desks or bookshelves in the room.

Fig. 20 exhibits the measured MEG's together with the calculated ones. The figure shows the average receiving powers measured when the human phantom was directed to 0°, 90°, 180°, and 270° relative to the tangential direction of the rotating arm. The average value for the four measurements is also shown. There is some discrepancy between the receiving powers in the four directions, implying that incident waves were nonuniform in azimuth. However, even in such a situation, it has been reported that the averaging process for the receiving power for azimuthally nonuniform incident waves agrees very well with that for a uniform model [23]. Thus, it is concluded that the measured result in Fig. 20 that should be compared with the analytical result is the average value of the four directions. The average values show a good agreement with the calculated ones, indicating that the analysis of MEG performed in this paper is made with adequately high accuracy.

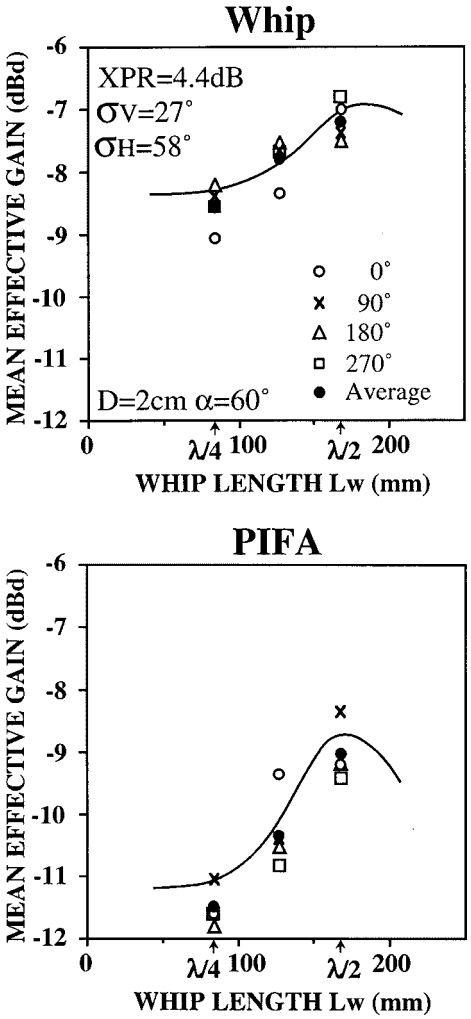

Fig. 20. Comparison between calculated and measured MEGs.

VII. Conclusion

The performance of a diversity antenna for portable telephones comprising a whip antenna and a planar inverted F antenna, which includes the electromagnetic effects of a human operator, has been analyzed. The analysis shows the radiation efficiency and mean effective gain as functions of whip length, head-to-radio separation, and body inclination angle from the vertical under various incident radiowave environments. These results will contribute to realizing stable and high-quality mobile radio communications.

Acknowledgment

The authors would like to thank Dr. M. Ando, professor of the Tokyo Institute of Technology, for his encouragement and support, Dr. T. Taga of the Nippon Telegraph & Telephone Corporation, and Dr. T. Uwano of the Central Research Laboratory of Matsushita Electric Co. Ltd. for their useful suggestions. The authors would also like to thank S. Ano for his efforts in measuring the various antenna models.

References

[1] K. Ogawa and T. Uwano, "A diversity antenna for very small 800-MHz band portable telephones," *IEEE Trans. Antennas Propagat.*, vol. 42, pp. 1342–1345, Sept. 1994.

[2] T. Taga, "Analysis for mean effective gain of mobile antennas in land mobile radio environments," *IEEE Trans. Veh. Technol.*, vol. 39, no. 2, pp. 117–131, 1990.

[3] K. Ogawa and T. Uwano, "Analysis of a diversity antenna comprising a whip antenna and a planar inverted-F-antenna for portable telephones" (in Japanese), *Trans. IEICE* , vol. J79-B-II, no. 12, pp. 1003–1012, Dec. 1996.

[4] ——, "Mean effective gain analysis of a diversity antenna for portable telephones in mobile radio communication environments" (in Japanese), *Trans. IEICE (B-II)*, vol. J81-B-II, no. 10, pp. 897–905, Oct. 1998.

[5] H. R. Chuang, "Human operator coupling effects on radiation characteristics of a portable communication dipole antenna," *IEEE Trans. Antennas Propagat.*, vol. 42, no. 4, pp. 556–560, Apr. 1994.

[6] K. Tsunekawa and A. Ando, "Advanced wire grid method for solving the scattered field of a lossy dielectric object," in *IEEE AP-S Int. Symp. Dig.*, July 1992, vol. 2, pp. 797–800.

[7] J. Toftgard, S. N. Hornsleth, and J. B. Andersen, "Effects on portable antennas of the presence of a person," *IEEE Trans. Antennas Propagat.*, vol. 41, no. 6, pp. 739–746, June 1993.

[8] K. Sato, K. Nishikawa, N. Suzuki, and A. Ogawa, "Analysis of antennas mounted on portable equipment near human body" (in Japanese), *Trans. IEICE (B-II)*, vol. J79-B-II, no. 11, pp. 892–900, Nov. 1996.

[9] M. A. Jensen and Y. Rahmat-Sami, "EM interaction of handset antennas and a human in personal communications," *Proc. IEEE*, vol. 83, pp. 7–17, Jan. 1995.

[10] S.-I. Watanabe, M. Taki, T. Nojima, and O. Fujiwara, "Characteristics of the SAR distributions in a head exposed to electromagnetic fields radiated by a hand-held portable radio," *IEEE Trans. Microwave Theory Tech.*, vol. 44, no. 10, pp. 1874–1883, Oct. 1996.

[11] K. Ogawa, T. Matsuyoshi, and K. Monma, "A study of the effects of the shoulder on the effective gain characteristics in the multiple radio wave environment of a dipole antenna close to a human head" (in Japanese), *Trans. IEICE (B)*, vol. J82-B, no. 10, pp. 1847–1856, Oct. 1999.

[12] H. Haruki and A. Kobayashi, "The inverted-F antenna for portable radio units" (in Japanese), in *Conv. Rec. IECE Jpn.*, Mar. 1982, p. 613.

[13] W. L. Stutzman and G. A. Thiele, *Antenna Theory and Design*. New York: Wiley, 1981, pp. 36–39.

[14] G. D. Vendelin, A. M. Pavio, and U. L. Rohde, *Microwave Circuit Design Using Linear and Nonlinear Techniques*. New York: Wiley, 1990, pp. 54–63.

[15] W. C. Jakes, *Microwave Mobile Communications*: IEEE Press, 1974, pp. 133–140.

[16] W. C. Y. Lee and R. H. Brandt, "The elevation angle of mobile radio signal arrival," *IEEE Trans. Commun.*, vol. COM-21, pp. 1194–1197, Nov. 1973.

[17] T. Kobayashi and T. Nojima, "Simulation of electromagnetic properties of biological tissues with solid and liquid materials and its applications," (in Japanese), , Tech. Rep. IEICE MW92-35, May 1992.

[18] K. Ogawa, T. Matsuyoshi, and K. Monma, "Antenna-pattern measurement at angles of signal arrival of portable radios near a human operator," in *APMC98 Int. Symp. Digest*, Dec. 1998, pp. 461–464.

[19] V. Hombach, K. Meier, M. Burkhardt, E. Kuhn, and N. Kuster, "The dependence of EM energy absorption upon human head modeling at 900 MHz," *IEEE Trans. Microwave Theory Tech.*, vol. 44, pp. 1865–1873, Oct. 1996.

[20] H. Arai, N. Igi, and H. Hanaoka, "Antenna-gain measurement of handheld terminals at 900 MHz," *IEEE Trans. Veh. Technol.*, vol. 46, pp. 537–543, Aug. 1997.

[21] T. Taga and K. Tsunekawa, "A built-in antenna for 800 MHz band portable radio units," in *Proc. ISAP '85*, 1985, pp. 425–428.

[22] T. Taga, "Indoor measurement method for evaluating statistical distribution of incident waves under out-of-sight condition and experimental studies of characteristics of mobile station polarization diversity" (in Japanese), *Trans. IEICE (B-II)*, vol. J74-B-II, no. 11, pp. 608–615, Nov. 1991.

[23] ——, "A study on mean effective gain of mobile antennas in effective line-of-sight propagation environments" (in Japanese), in *Conv. Rec. IEICE Japan*, Mar. 1990, pp. 2–23.

[24] K. Ogawa and T. Uwano, "Analysis of a diversity antenna comprising a whip antenna and a planar inverted-F-antenna for portable telephones," *Electron. Commun. Japan*, pt. 1, vol. 80, no. 8, pp. 39–49, 1997.

[25] ——, "Mean effective gain analysis of a diversity antenna for portable telephones in mobile radio communication environments," *Electron. Commun. Japan*, pt. 1, vol. 83, no. 3, pp. 88–97, 2000.

[26] K. Sato, K. Nishikawa, N. Suzuki, and A. Ogawa, "Analysis of antennas mounted on portable equipment near human body," *Electron. Commun. Japan*, pt. 1, vol. 80, no. 11, pp. 54–63, 1997.

[27] K. Ogawa, T. Matsuyoshi, and K. Monma, "A study of the effects of the shoulder on the effective gain characteristics in the multiple radio wave environment of a dipole antenna close to a human head-F-antenna for portable telephones," *Electron. Commun. Japan*, pt. 1, vol. 84, no. 1, pp. 21–30, 2001.

Koichi Ogawa (M'89) was born in Kyoto, Japan, on May 28, 1955. He received the B.S. and M.S. degrees in electrical engineering from Shizuoka University, Japan, in 1979 and 1981, respectively, and the Dr.E. degree in electrical engineering from Tokyo Institute of Technology, Tokyo, Japan, in 2000.

He joined Matsushita Electric Industrial Company, Ltd., Osaka, Japan, in 1981, where he was engaged in research and development work on a 50-GHz millimeter-wave integrated circuit and a 12/14-GHz very small aperture terminal (VSAT) satellite communication system. He is currently a Research Group Leader of Mobile Communication RF-Devices. His research interests include diversity antennas for portable handsets, compact antennas for mobile communication systems, and other related areas of radio propagation.

Dr. Ogawa received the OHM Technology Award from the Promotion Foundation for Electrical Science and Engineering in 1990. He also received the TELECOM Systems Technology Award from the Telecommunications Advancement Foundation (TAF) in 2001. He was a member of the Institute of Electronics, Information and Communication Engineers (IEICE) of Japan Committee on Electromagnetic Human Phantom. He was a Chairman of the technical session for antenna human interactions at the IEEE AP-S'99 International Symposium, Orlando, FL. He also chaired technical sessions for mobile station antennas/ human interactions with mobile communication antennas at the IEEE VTC2000 and IEICE ISAP2000 International Symposiums in Japan. He is listed in *Who's Who in the World*.

Toshimitsu Matsuyoshi was born in Hyogo, Japan, on February 10, 1970. He received the B.S. and M.S. degrees in communication engineering from Osaka University, Osaka, Japan, in 1992 and 1994, respectively.

He joined Matsushita Electric Industrial Company, Ltd., Osaka, in 1994 and has been engaged in research and development work on microwave filters and amplifiers. He is presently engaged in research and development on antennas for mobile communication systems.

Mr. Matsuyoshi is a member of the Institute of Electronics, Information and Communication Engineers (IEICE) of Japan.

Kenji Monma was born in Kanagawa, Japan, on August 27, 1973. He received the B.S. degree in communication engineering from Tohoku University, Sendai, Japan, in 1996.

He joined Matsushita Electric Industrial Company, Ltd., Osaka, Japan, in 1996 and has been engaged in research and development work on microwave circuits and antennas for mobile communication systems.